Earth and Planetary Science Letters 432 (2015) 342–353

Contents lists available at ScienceDirect

Earth and Planetary Science Letters

www.elsevier.com/locate/epsl

Distal and proximal controls on the silicon stable isotope signature of North Atlantic Deep Water

Gregory F. de Souza [a,b,*], Richard D. Slater [a], Mathis P. Hain [c], Mark A. Brzezinski [d], Jorge L. Sarmiento [a]

[a] Program in Atmospheric and Oceanic Sciences, Princeton University, Princeton, NJ 08544, USA
[b] ETH Zurich, Institute of Geochemistry and Petrology, NW C81.3, Clausiusstrasse 25, 8092 Zurich, Switzerland
[c] National Oceanography Centre, University of Southampton, Southampton SO14 3ZH, UK
[d] Marine Science Institute, University of California, Santa Barbara, CA 93106, USA

ARTICLE INFO

Article history:
Received 19 July 2015
Received in revised form 11 October 2015
Accepted 18 October 2015
Available online xxxx
Editor: H. Stoll

Keywords:
biogeochemical cycles
silicon isotopes
meridional overturning circulation

ABSTRACT

It has been suggested that the uniquely high δ^{30}Si signature of North Atlantic Deep Water (NADW) results from the contribution of isotopically fractionated silicic acid by mode and intermediate waters that are formed in the Southern Ocean and transported to the North Atlantic within the upper limb of the meridional overturning circulation (MOC). Here, we test this hypothesis in a suite of ocean general circulation models (OGCMs) with widely varying MOCs and related pathways of nutrient supply to the upper ocean. Despite their differing MOC pathways, all models reproduce the observation of a high δ^{30}Si signature in NADW, as well showing a major or dominant (46–62%) contribution from Southern Ocean mode/intermediate waters to its Si inventory. These models thus confirm that the δ^{30}Si signature of NADW does indeed owe its existence primarily to the large-scale transport of a distal fractionation signal created in the surface Southern Ocean. However, we also find that more proximal fractionation of Si upwelled to the surface within the Atlantic Ocean must also play some role, contributing 20–46% of the deep Atlantic δ^{30}Si gradient. Finally, the model suite reveals compensatory effects in the mechanisms contributing to the high δ^{30}Si signature of NADW, whereby less export of high-δ^{30}Si mode/intermediate waters to the North Atlantic is compensated by production of a high-δ^{30}Si signal during transport to the NADW formation region. This trade-off decouples the δ^{30}Si signature of NADW from the pathways of deep water upwelling associated with the MOC. Thus, whilst our study affirms the importance of cross-equatorial transport of Southern Ocean-sourced Si in producing the unique δ^{30}Si signature of NADW, it also shows that the presence of a deep Atlantic δ^{30}Si gradient does not uniquely constrain the pathways by which deep waters are returned to the upper ocean.

1. Introduction

1.1. Marine Si cycling and the δ^{30}Si distribution

The cycling of nutrients in the sea is determined by a complex set of interactions between biota in the surface ocean and the physical circulation across a range of spatial and temporal scales. At the global scale, the export of nutrients to the abyss in biogenic particles is balanced by the supply of dissolved nutrients via the upwelling of nutrient-rich deep waters in the MOC (Broecker and Peng, 1982; Sarmiento et al., 2007). At the scale of the thermocline, nutrient distributions are determined by how the location and timing of biological nutrient drawdown at the surface interacts with the subduction of water masses and their gyre- to basin-scale circulation (Sarmiento et al., 2004; Palter et al., 2005; Karleskind et al., 2011). These distributions in turn determine the magnitude, biogeography and distribution of low-latitude primary productivity (Marinov et al., 2006; Palter et al., 2010, 2011). The ocean interior distributions of nutrients thus both influence and are influenced by biological productivity, and bear the imprint of the interaction between productivity and the ocean's three-dimensional circulation, allowing them to be used to infer the physical and biological interactions that determine marine nutrient cycling. This study takes such an approach in order to trace the influence of physical–biological interactions on the large-scale transports associated with the marine cycle of silicon (Si).

* Corresponding author at: ETH Zurich, Institute of Geochemistry and Petrology, NW C81.3, Clausiusstrasse 25, 8092 Zurich, Switzerland. Tel.: +41 44 632 6983.
E-mail address: desouza@erdw.ethz.ch (G.F. de Souza).

http://dx.doi.org/10.1016/j.epsl.2015.10.025
0012-821X/

Of the ocean's photosynthesizing primary producers, diatoms are the most important group for the export of organic carbon from the surface ocean (e.g. Buesseler, 1998). As a result, they play a key role in the biological pump, a mechanism by which the ocean modulates atmospheric pCO_2 (Hain et al., 2014a). Whilst their opaline cell wall, or frustule, provides diatoms protection from predators (Smetacek, 1999) and is less energy-intensive to produce than an organic cell wall (Raven, 1983), it also makes them vitally dependent on the presence of Si dissolved in seawater. The boom-bust behavior of diatom populations that leads to their importance for carbon export also means that diatoms are very efficient exporters of Si to depth (Brzezinski et al., 2003), such that they are the main driver of marine Si cycling (Tréguer and De la Rocha, 2013). Diatom uptake of Si discriminates between its isotopes, with lighter Si isotopes being preferentially incorporated into the frustule (De la Rocha et al., 1997; Sutton et al., 2013), leaving the residual Si in seawater enriched in heavier Si isotopes. Diatom Si uptake at the ocean's surface thus produces a signal of biological cycling in the stable isotope composition of seawater Si (expressed in the standard delta notation as δ^{30}Si), which can be used as a tracer of the marine Si cycle (e.g. Cardinal et al., 2005; Reynolds et al., 2006; Beucher et al., 2008; de Souza et al., 2012a; Grasse et al., 2013). For instance, diatom uptake in the surface Southern Ocean produces elevated δ^{30}Si in the deep winter mixed layers from which the Southern Ocean mode/intermediate water masses Subantarctic Mode Water (SAMW) and Antarctic Intermediate Water (AAIW) are ventilated (Fripiat et al., 2011). This isotopic signal is transported into the subtropical interior by the spreading of these water masses from their formation regions (de Souza et al., 2012b).

The clearest large-scale signal in the marine δ^{30}Si distribution is the δ^{30}Si gradient in the deep Atlantic Ocean (Fig. 1a; de Souza et al., 2012a; Brzezinski and Jones, 2015), with a systematic trend from high δ^{30}Si values in deep waters of the Si-poor North Atlantic, influenced by NADW, to lower values towards the Si-richer south, influenced by Antarctic Bottom Water (AABW). This coherent gradient is related to the quasi-conservative mixing of Si between these two water masses (Broecker et al., 1991), as reflected by the systematics (Fig. 1a) and water-column distribution (Fig. 1b) of δ^{30}Si in the Atlantic, both of which indicate water-mass control on the δ^{30}Si distribution. de Souza et al. (2012a) suggested that the high δ^{30}Si value of NADW ultimately results from the creation of a high-δ^{30}Si signal by diatom Si uptake in the surface Southern Ocean, a signal that is transported to the North Atlantic by SAMW/AAIW in the upper limb of the MOC. This mechanism has since been invoked to explain the isotope distributions of other biogeochemically-cycled elements, such as cadmium (e.g. Abouchami et al., 2014).

Such a Southern-Ocean-focused mechanism is consistent with burgeoning evidence that the dominant MOC pathway by which dense and nutrient-rich deep waters are brought to the surface is the wind-driven upwelling in the Southern Ocean (Toggweiler and Samuels, 1993; Sarmiento et al., 2004; Lumpkin and Speer, 2007; Marshall and Speer, 2012; Morrison et al., 2015), contrary to the canonical view of upwelling through the low-latitude thermocline (Robinson and Stommel, 1959; Broecker and Peng, 1982). However, some recent observationally-based estimates of global overturning indicate a significant role of low-latitude upwelling in closing the MOC (Talley et al., 2003; Talley, 2008). By using numerical ocean models to examine the relationship between the NADW δ^{30}Si signature and the pathways by which Si is transported by the MOC, this study assesses de Souza et al.'s (2012a) hypothesis of large-scale controls on the Atlantic δ^{30}Si distribution, whilst also considering the constraints placed by these observations on pathways of upwelling associated with the MOC.

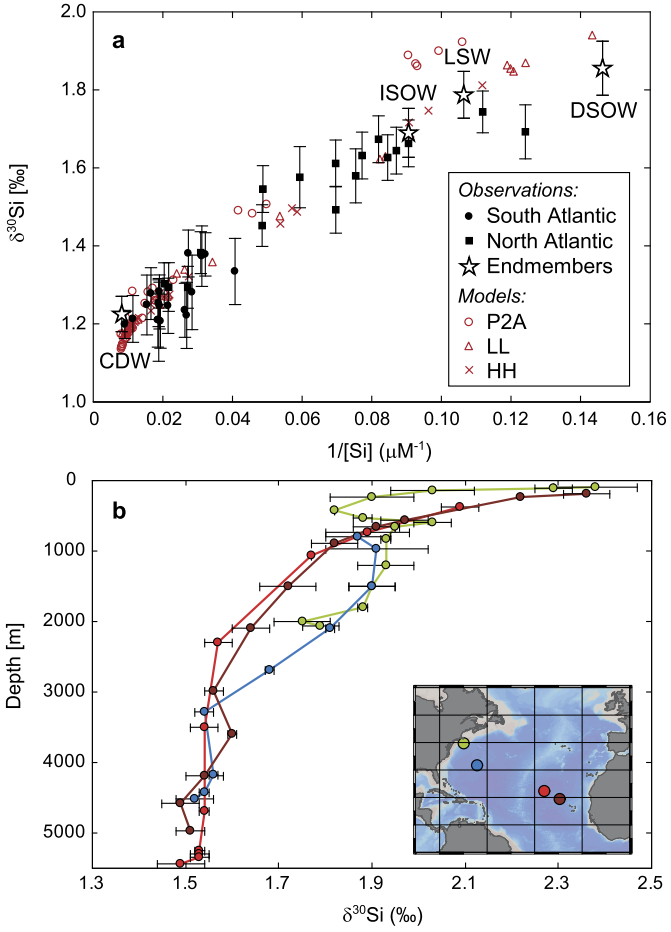

Fig. 1. Silicon isotope data from the Atlantic Ocean. (a) Data from the deep (>2000 m) Atlantic Ocean from latitudes ranging from ~60°N to ~60°S in isotope mixing space (de Souza et al., 2012a), illustrating the systematic variation of deep water δ^{30}Si values. The near-linear relationship between δ^{30}Si and 1/[Si] indicates quasi-conservative mixing of Si brought into the deep Atlantic by Si-rich Southern Ocean sources (CDW) as well as Si-poor North Atlantic (LSW) and Nordic (DSOW, ISOW) sources. Open red symbols are results from the OGCMs used in this study (see Section 2.1), subsampled at the observational sampling locations. (b) Depth profiles of δ^{30}Si from the GEOTRACES North Atlantic Zonal Transect at 20°–40°N (Brzezinski and Jones, 2015) reveal the elevated δ^{30}Si values associated with the southward transport of NADW at mid-depths in the western Atlantic Ocean (blue and green points; see inset). (For interpretation of the references to color in this figure legend, the reader is referred to the web version of this article.)

1.2. Support for a Southern Ocean control

Support for a Southern Ocean control on the NADW δ^{30}Si signature is provided by the model CYCLOPS, an ocean box model originally developed by Keir (1988) that has been modified to explicitly represent the physical and biogeochemical zonation of the surface Southern Ocean (Fig. 2a; Robinson et al., 2005; Hain et al., 2014b). A representation of the marine cycling of Si and its isotopes (see Supplementary Information) allows an assessment of the leading-order sensitivities of the large-scale δ^{30}Si distribution. As shown in Fig. 2b, the observed deep Atlantic Si concentration gradient (~110 μM) can be reproduced by simultaneously varying the length-scale defining the dissolution of opal export (which determines the partitioning of opal dissolution between the intermediate and deep ocean) and the degree of Si drawdown in the Subantarctic Zone (SAZ), from where the model's Southern Ocean mode/intermediate waters are ventilated. In contrast, the gradient in δ^{30}Si between NADW and the deep Southern Ocean is mostly insensitive to the opal dissolution length-scale, but varies systematically with Si drawdown in the SAZ, disappear-

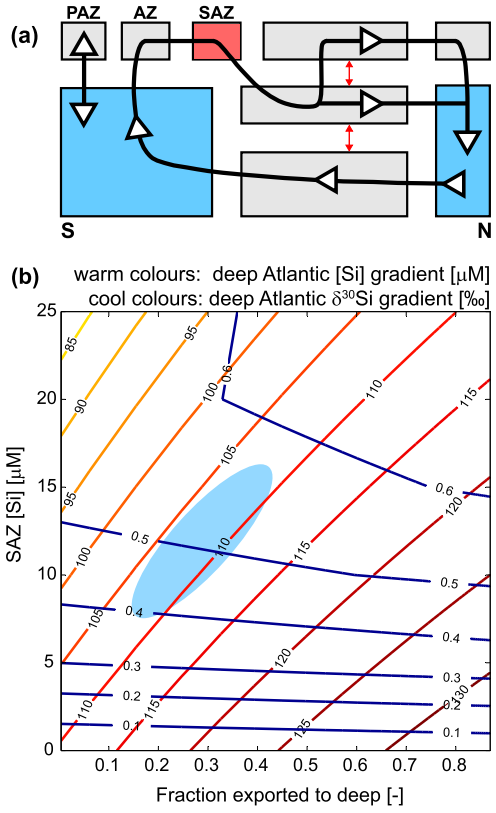

Fig. 2. (a) Schematic representation of the Atlantic circulation in the CYCLOPS ocean box model (Hain et al., 2014b), highlighting advective transport (black arrows) and diffusive exchange (red arrows) fluxes. In the sensitivity study discussed in the text (Section 1.2), the Si concentration of the Subantarctic surface box (light red shading) was systematically varied together with the length scale of opal dissolution, which controls the fraction of the sinking opal flux exported to the deep ocean boxes. The results of these parameter variations on the deep Atlantic [Si] and δ^{30}Si gradients (calculated as the difference between the deep high-latitude boxes; light blue shading) is shown in panel *b* (warm colours: Δ[Si] in μM; cool colours: $\Delta\delta^{30}$Si in ‰). PAZ: polar Antarctic zone; AZ: Antarctic zone. The light blue shaded region in panel *b* corresponds to observations (Δ[Si] $\sim$ 108 μM, $\Delta\delta^{30}$Si $\sim$ 0.5‰). (For interpretation of the references to color in this figure legend, the reader is referred to the web version of this article.)

ing when the Si concentration in the SAZ is forced to zero, so as not to leave any residual high-δ^{30}Si in the SAZ surface (Fig. 2b). Under these conditions, the model's advective pathway of Si supply from the surface Southern Ocean to the high-latitude North Atlantic via mode/intermediate waters has been entirely eliminated, such that Si can reach the North Atlantic solely via diffusive upward supply from the low-latitude deep ocean. This sensitivity of the Atlantic δ^{30}Si gradient to Si supply by mode/intermediate waters supports the hypothesis that it results from the cross-equatorial transport of a partial Si consumption signal from the surface Southern Ocean. In the following, we further test this hypothesis by explicitly tracing the origins of Si supplied to the North Atlantic by the large-scale ocean circulation in a suite of OGCMs in which the pathways of deep water upwelling associated with the MOC are systematically varied.

1.3. A theoretical framework

Gnanadesikan's (1999; hereafter G99) analytical model of the volume balance of the oceanic pycnocline (Fig. 3a) provides the conceptual basis for the OGCM suite presented in this study. This model shows that the depth D of the pycnocline, separating the buoyant waters of the upper ocean from the dense waters of the deep, results from the balance between four key processes that add or remove buoyant water from the upper ocean. These processes are (i) the formation of deep water in the North Atlantic (T_n in Fig. 3a), the balance between (ii) wind-driven upwelling and northward Ekman transport in the Southern Ocean (T_w) and (iii) southward eddy-induced advection of light waters (T_e), and (iv) low-latitude upwelling through the thermocline (T_u). There are two pathways by which volume lost from the upper ocean during NADW formation can be replaced: (a) downward heat transport driven by diapycnal mixing lightens dense waters, leading to an upwelling flux through the thermocline; (b) Ekman divergence in the Southern Ocean drives the adiabatic upwelling of deep waters, which are converted to lighter waters at the surface. G99 showed that the partitioning of upwelling between these two pathways depends on diapycnal mixing and the advective effects of eddies, represented by the diapycnal and isopycnal eddy diffusivities (κ_v and A_I) respectively. When these diffusivities are small, both low-latitude upwelling T_u and the eddy return flow T_e compensating northward Ekman transport T_w are minimal, such that deep upwelling (and the associated nutrient supply) is driven by Ekman divergence in the surface Southern Ocean T_w (Fig. 3a). If, on the other hand, A_I is large enough that the southward advective eddy transport in the Southern Ocean largely compensates northward Ekman transport (i.e. if the net flux $T_w - T_e$ is small), most upwelling takes place at low latitudes (T_u). This simultaneously requires high κ_v in order to maintain the observed depth of the pycnocline against a large upwelling flux. This simple model thus makes an important point: the pathway by which dissolved nutrients stored in the deep ocean return to the surface depends on the vigorousness of turbulent mixing across and along density surfaces. By varying both these parameters simultaneously in a numerical ocean model, we can produce widely varying pathways of upwelling whilst maintaining the observed depth of the

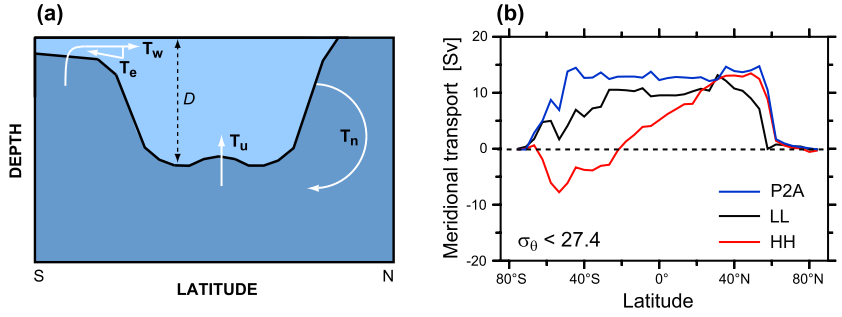

Fig. 3. (a) Theoretical model framework of Gnanadesikan (1999) and (b) northward meridional volume transport above the $\sigma_\theta = 27.4$ isopycnal in the suite of OGCMs used in this study, whose construction is based on the theory of Gnanadesikan (1999). In panel *a*, the depth D of the pycnocline (light blue shading) is maintained by the volume balance between flux T_n representing sinking of dense water in the North Atlantic, T_u representing low-latitude upwelling, and the balance between wind-driven northward Ekman transport T_w and eddy-induced southward transport T_e in the Southern Ocean. (For interpretation of the references to color in this figure legend, the reader is referred to the web version of this article.)

ocean's pycnocline. This study utilizes three variants of an OGCM with differing MOC pathways in order to systematically examine the relationship between the δ^{30}Si signature of NADW and large-scale Si transport.

2. Methods

2.1. Model description and setup

The physical ocean model used is the Modular Ocean Model 3.0 (MOM3; Pacanowski and Griffies, 1999), run at 3.75° × 4.5° horizontal resolution with 24 vertical levels. This primitive-equation OGCM forms the basis of a model suite in which the values of diapycnal and isopycnal diffusivity are systematically varied according to the theory of G99, so as to produce varying MOC pathways. This suite is described in detail by Gnanadesikan et al. (2002, 2004, 2007) and Palter et al. (2010). In this study, we employ model variants LL, HH and P2A, whose key variables are summarized in Table S1. Model variant LL is a version of MOM3 in which both diapycnal and isopycnal eddy diffusivities have low values. In LL, κ_v in the pycnocline is 1.5×10^{-5} m^2/s, similar to values inferred from direct tracer release experiments (Ledwell et al., 1993, 1998), increasing to 1.3×10^{-4} m^2/s at depth with a hyperbolic tangent transition at 2500 m. Isopycnal diffusivity A_I, which is also the coefficient used in the models' Gent–McWilliams parameterization of eddy thickness diffusion (Gent et al., 1995), has a constant value of 1000 m^2/s in LL. In model variant HH, in contrast, both κ_v and A_I have high values: at 6×10^{-5} m$^2/s$, pycnocline κ_v is four times higher than in LL, whilst the A_I of 2000 m^2/s is twice as large as in LL. Finally, model variant P2A conforms to observational constraints of low pycnocline diffusivity (and thus has a pycnocline κ_v of 1.5×10^{-5} m^2/s and A_I of 1000 m^2/s, as in LL), but simulates increased diapycnal mixing in the Southern Ocean, motivated by observations of high internal wave activity there (Polzin et al., 1997). In addition to a number of specific changes relative to LL as listed in Table S1 (and discussed by de Souza et al., 2014), P2A is forced by the ECMWF atmospheric reanalysis of Trenberth et al. (1989), which imposes higher wind stresses over the Southern Ocean than the reanalysis that forces LL and HH (Hellerman and Rosenstein, 1983).

The physical models are coupled to the nutrient-restoring biogeochemical model of Jin et al. (2006), modified by de Souza et al. (2014) to include Si isotopes. As discussed therein, the model simulates isotope fractionation during Si uptake in the surface ocean, but does not fractionate Si isotopes during opal dissolution (Demarest et al., 2009; Wetzel et al., 2014; for a detailed discussion of this issue see de Souza et al., 2014). Further diagnostics added for this study (Section 2.2) allow us to trace Si originating from four high-latitude source regions in the models.

The simulations are initialized to steady-state physical conditions and distributions of Si and δ^{30}Si from a 5000-yr spin-up simulation for each model variant. The fractional contribution of each of the four source regions (Section 2.2) to the Si inventory is initialized to a globally constant value of 25%, and the simulations run forward for 2000 model years, by which time the Si source tracer distributions achieve equilibrium. Targets for surface nutrient restoring are derived from the objectively-analyzed monthly climatologies of World Ocean Atlas 2009 (WOA09; Garcia et al., 2010). Results of the simulations are presented as averages over the last 20 yrs of the simulations. We also present the models' equilibrium (pre-bomb) radiocarbon distributions (Δ^{14}C; Matsumoto et al., 2004) as 10-yr means.

2.2. Si source tagging scheme

In order to study the large-scale Si dynamics and transport in the model variants, we explicitly trace four sources of Si, using the method of Palter et al. (2010). As defined in Fig. 4, we tag and trace Si sourced from (a) the region of SAMW formation (*SAMW*), (b) the region of AAIW formation (*AAIW*), (c) the deep Southern Ocean (*DEEP*), and (d) the subpolar North Pacific Ocean (*NPAC*). At every model time step, Si within a defined source region is 'tagged' with the corresponding source identity. For example, AAIW-derived Si is tagged between the $\sigma_\theta = 27.1$ and $\sigma_\theta = 27.4$ isopycnals south of where the $\sigma_\theta = 26.5$ isopycnal shoals to 200 m (see Fig. 4). Si tagged in this manner is transported away from its source region by the circulation, and retains its source identity as it cycles through the low latitude ocean and into the North Atlantic, our region of interest. Once acquired, source identity is only destroyed when Si enters another source region: e.g., AAIW-derived Si flowing northward in the surface Southern Ocean will lose its AAIW identity and be tagged as SAMW-sourced Si once it crosses the instantaneous outcrop of the $\sigma_\theta = 27.1$ isopycnal. The sum of all four source tracers equals the total pool of Si, allowing us to trace the fractional contribution of the source regions to the local Si inventory at any point in the model. In the following, we refer to Si that has been tagged with a particular source identity as being 'sourced' or 'derived' from that region (e.g. 'SAMW-derived').

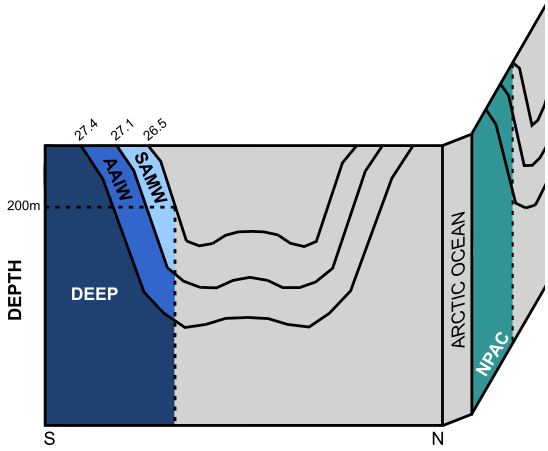

Fig. 4. Schematic meridional Atlantic section showing the tagging scheme employed to trace Si sources to the North Atlantic Ocean. Curved black lines represent potential density anomaly (σ_θ) surfaces labeled at their southern outcrop. Each coloured area represents a tagging region within which Si is assigned a source "identity". Four sources of Si are traced: SAMW, AAIW, deep Southern Ocean (*DEEP*) and North Pacific (*NPAC*). The southern hemisphere tagging regions are circumpolar, whilst the NPAC tagging region is restricted to the North Pacific Ocean. The identity of Si tagged in any one region is destroyed when it enters another coloured tagging region, where it is assigned a new source identity. Within the gray area, tagged Si is cycled by biology and transported by the physical circulation analogously to the total Si pool.

3. Results

3.1. MOC pathways, Si and δ^{30}Si distributions

We begin by describing the upwelling pathways of the three model variants. Fig. 3b shows the zonally-averaged northward meridional volume transport above the $\sigma_\theta = 27.4$ isopycnal, which lies at a depth of 800–1000 m at low latitudes in all models. An increase in horizontal transport implies upwelling of water across this density surface, into the upper ocean. Thus, the differing latitudinal evolution of this transport in the models reflects their differing MOC pathways. The constancy of P2A's meridional transport north of ~50°S shows that this model achieves most of its upwelling at high southern latitudes (Fig. 3b). This Southern Ocean upwelling pathway is expected from G99 (Fig. 3a), given the low isopycnal and diapycnal diffusivities and the strong winds over the Southern Ocean (Table S1): P2A not only restricts T_u through lim-

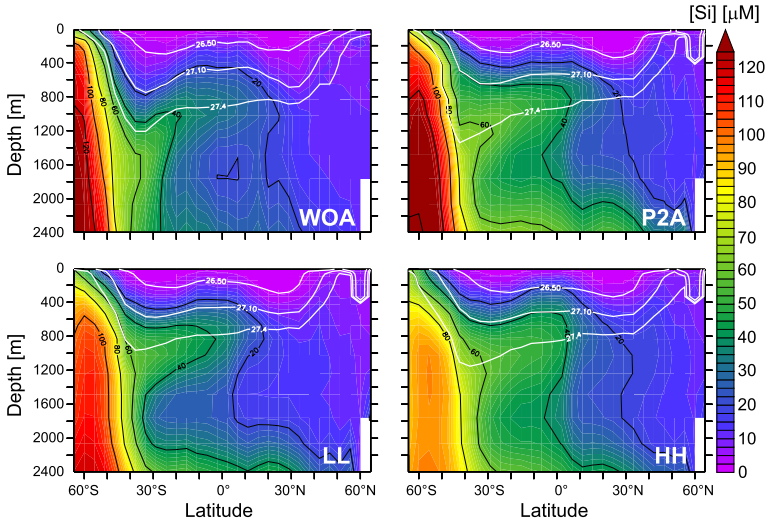

Fig. 5. Meridional sections showing the Atlantic-mean Si distribution in the uppermost 2400 m in World Ocean Atlas 2009 (upper left) and the three model variants. Concentrations are averaged over the Atlantic basin, and over the Southern Ocean from 60°W to 30°E.

ited low-latitude diapycnal mixing and T_e through low isopycnal diffusivity, but also has high T_w as a result of stronger Ekman transport in the Southern Ocean. In contrast, volume transport in HH increases over a wide latitudinal band from ∼50°S to ∼30°N, reflecting low-latitude upwelling. The importance of low-latitude transport (T_u) for the overturning is expected from G99, given HH's high diffusivities and weaker Southern Ocean winds. Model variant LL is intermediate between these two extremes, since southern upwelling extends further north than in P2A, but limited low-latitude upwelling is implied by the constancy of meridional volume transport north of ∼30°S. The overturning pathways simulated by LL and P2A are more consistent with estimates from inverse models (Lumpkin and Speer, 2007) and the emerging view of ocean overturning (Marshall and Speer, 2012; Talley, 2013), although LL's ventilation of the deep Southern and Pacific Oceans is too sluggish to accurately reproduce the $\Delta^{14}C$ distribution (Matsumoto et al., 2004).

When combined with their shared biogeochemical model, which restores surface Si concentrations towards observations, the circulation fields of the three models produce interior Si distributions that reproduce the large-scale structure to the observed distribution, but also show differences both from the observations and from each other. Fig. 5 compares the models' average Atlantic Si distribution in the uppermost 2400 m with WOA09 (see Fig. S3 for zonal averages). As in the observations, all models exhibit a southward propagating tongue of low-Si NADW at mid-depth, and an intermediate-depth tongue of elevated Si extending northwards from the Southern Ocean. However, in all model variants, the low-Si tongue is too shallow, with a core at ∼1600 m rather than ∼1800 m as in the observations. This is because North Atlantic convection in the models produces a water mass that is too light and thus descends to shallower depths than observed. As a result, the models' Si-rich AABW extends too far north, and upward diapycnal mixing of Si from this water mass leads to the elevated Si concentrations seen below ∼2200 m in all model variants. All models also overestimate Si in the northward-penetrating intermediate-depth tongue, a feature that is more pronounced in P2A and HH than in LL. The Si distribution of HH is least similar to the observations: the southward- and northward-propagating advective signals are much less clearly defined in this model than in LL or P2A, due to high interior diapycnal mixing. Model HH also strongly underestimates Si concentrations in the deep Southern Ocean relative to observations.

Despite these differences in the Si distribution between models, they display similar skill at reproducing the interior Atlantic δ^{30}Si distribution, especially in terms of its isotope systematics: as shown by Fig. 1a, all three models reproduce the near-linear δ^{30}Si–1/Si relationship observed in the deep Atlantic Ocean, simulate a similar range of δ^{30}Si variation in Atlantic deep waters, and reproduce the observation of elevated δ^{30}Si in the Si-poor deep North Atlantic. We will discuss the reasons for these similarities in Section 4. For now, bearing the differences in the Si distribution of the three models in mind, in the following we discuss the Si source tracer distributions in terms of their *fractional* contribution to the total Si inventory, $f(i) = [\mathrm{Si}]_{\mathrm{source}=i} / \sum_j [\mathrm{Si}]_{\mathrm{source}=j}$.

3.2. Si source tracer distributions

By examining the steady-state distributions of the Si source tracer contributions $f(i)$, we can study how Si from the four source regions spreads through the ocean to eventually contribute to the NADW Si inventory. We illustrate the influence of the models' differing MOC pathways on large-scale Si transport by examining the contribution of each source region to the Si inventory of the thermocline, which we define as the volume of water above the $\sigma_\theta = 26.8$ isopycnal.

The two sources of Si above the $\sigma_\theta = 26.8$ isopycnal, SAMW and NPAC, exhibit their maximal contributions to the thermocline Si inventory close to their source regions, from where Si is directly introduced into the thermocline (Fig. 6). The locus of maximum fraction of SAMW-derived Si, f(SAMW), follows typical SAMW ventilation pathways (Sallée et al., 2010), extending anti-clockwise into the subtropics from the southern outcrop (Fig. 6a). NPAC-sourced Si enters the North Pacific thermocline from the north (Fig. 6d), and is transported into the Indian Ocean via the Indonesian Throughflow, although virtually none enters the Atlantic via the warm-water pathway (Gordon, 1986) without first entering the SAMW source region and losing its NPAC identity. NPAC-derived Si also flows northward through Bering Strait, contributing considerably to the Si inventory of the Arctic Ocean above $\sigma_\theta = 26.8$.

Silicon sourced from below the $\sigma_\theta = 26.8$ isopycnal (AAIW and DEEP) exhibits rather different thermocline distributions, since it can enter the thermocline only via interior diapycnal fluxes across this isopycnal. Thus, the contribution of AAIW- and DEEP-sourced Si increases towards the subtropics and tropics, as deeper-lying Si is transported upwards (Fig. 6b, c). In concordance with the models' differing MOC pathways, the contribution of DEEP-sourced Si

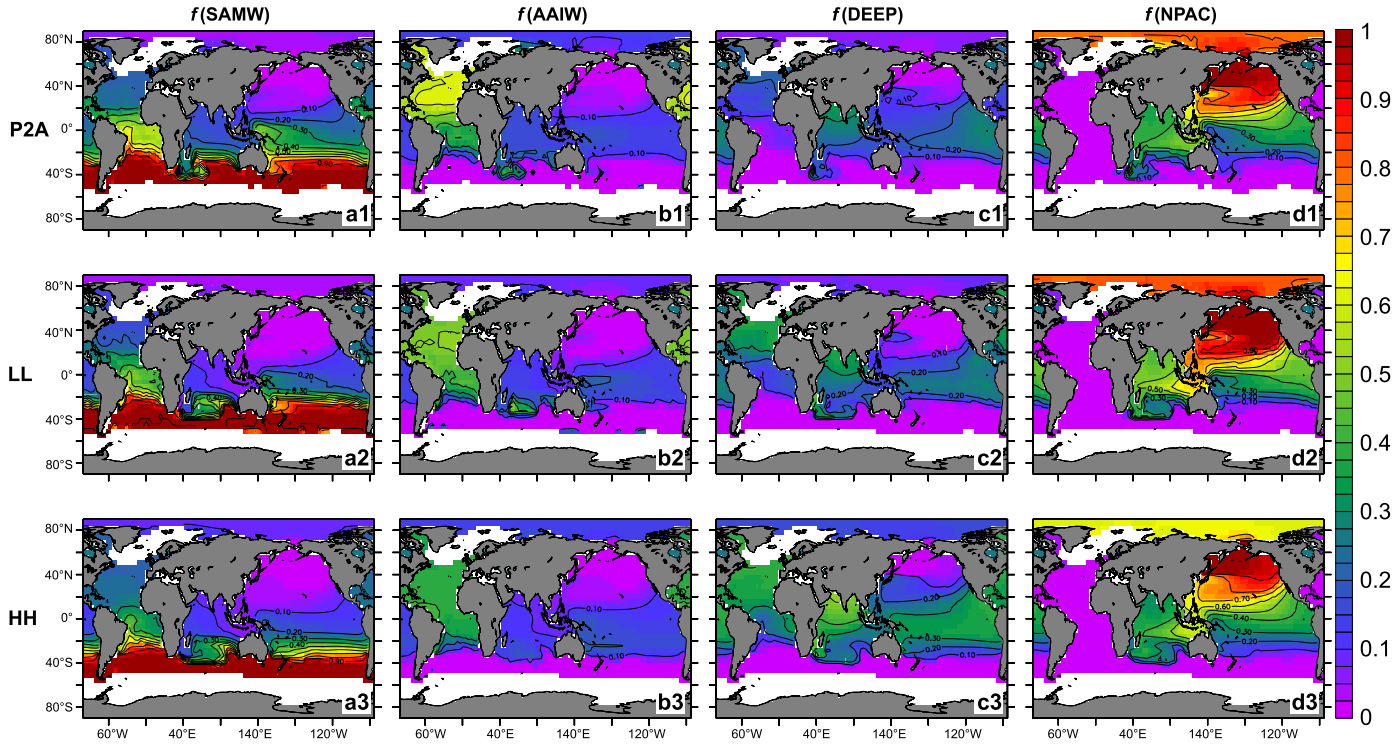

Fig. 6. Contribution of each source region to the Si inventory of the thermocline ($\sigma_\theta < 26.8$) in the three model variants [mol Si/mol Si, unitless]. White shading indicates the absence of water lighter than $\sigma_\theta = 26.8$.

to the thermocline inventory is highest in the diffusive model HH, and is lowest in the more adiabatic P2A, whose thermocline is also more vigorously ventilated along isopycnals from the south due to higher wind stress over the Southern Ocean. The contribution of DEEP-sourced Si to the thermocline inventory is 1.3–1.6 times higher in HH than in LL or P2A in the low-latitude Indian and Pacific Oceans, and even higher in the Atlantic, where it can be more than twice as large in HH than in P2A (Fig. 6c). Complementarily, high contributions of SAMW- and AAIW-derived Si penetrate further northward in LL and P2A than in HH: high contributions of SAMW-derived Si extend well into the North Atlantic in LL and P2A, such that f(SAMW) is 1.3–1.7 times higher in the tropical Atlantic thermocline of these models than in HH (Fig. 6a). Additionally, the fraction of AAIW-derived Si in the Atlantic thermocline increases steadily towards the north in LL and P2A but not in HH, such that in the North Atlantic subtropics, f(AAIW) in P2A and LL is 1.2–1.5 times higher than in HH (Fig. 6b). In all three models, however, SAMW- and AAIW-sourced Si together contribute at least half the Si inventory of the North Atlantic thermocline.

3.3. Diapycnal Si redistribution in the Atlantic Ocean

The consequences of northward transport of SAMW- and AAIW-derived Si for the source composition of NADW are illustrated by Fig. 7, which shows the average source tracer contributions $f(i)$ in the uppermost 2400 m of the Atlantic Ocean (see Fig. S4 for zonal averages). Only SAMW-derived Si spreads northwards at the surface, whilst Si from other source regions enters the Atlantic within the interior. Diapycnal processes and biological cycling disperse Si from all four source regions through the water column, e.g. the upward transport of DEEP-sourced Si into the thermocline, seen most strongly in HH (Fig. 7c). However, diapycnal Si redistribution is reflected most dramatically by the two source tracers that are tagged in the upper ocean according to density criteria, i.e. SAMW and AAIW. The downward penetration of Si from these sources is greatest in the North Atlantic north of 40°N (Fig. 7a, b). A tongue of elevated f(SAMW) and f(AAIW) propagates southwards from these high latitudes at about 1500–1600 m, at densities significantly higher than those at which these tracers are originally tagged (Fig. S5). This mid-depth tongue is the signal of NADW (Fig. 5), and reflects the diapycnal transfer of Si sourced from the shallow Southern Ocean to deep water densities, due to buoyancy loss in the subpolar North Atlantic, the Nordic Seas and the Arctic Ocean. The incorporation of SAMW- and AAIW-derived Si into NADW takes place in all three model variants, although their importance for its Si inventory varies, due to the differing extent of their transport to the shallow North Atlantic. All three models also exhibit a deep (~1800 m) tongue of NPAC-sourced Si extending southwards from the subpolar North Atlantic (Fig. 7d). This is Si that has been transported from the North Pacific via the Arctic Ocean, entering the North Atlantic through the models' representation of the Nordic Sea overflows.

4. Discussion

The Si source tracer distributions reveal the pathways of large-scale Si transport and diapycnal redistribution in the Atlantic Ocean. In the following, we focus on NADW flowing southward from the subpolar North Atlantic, in order to elucidate the processes responsible for its unique δ^{30}Si signature.

4.1. The isotopic signatures and source composition of NADW

As indicated by the simulated Atlantic δ^{30}Si systematics (Fig. 1a), which show elevated δ^{30}Si values associated with Si-poor waters of the deep North Atlantic, NADW appears prominently in the simulated δ^{30}Si distribution as a high-δ^{30}Si tongue along the western boundary of the mid-depth North Atlantic in all three models (Fig. 8a). The basin-scale structure of the simulated δ^{30}Si distributions is broadly consistent with observations of

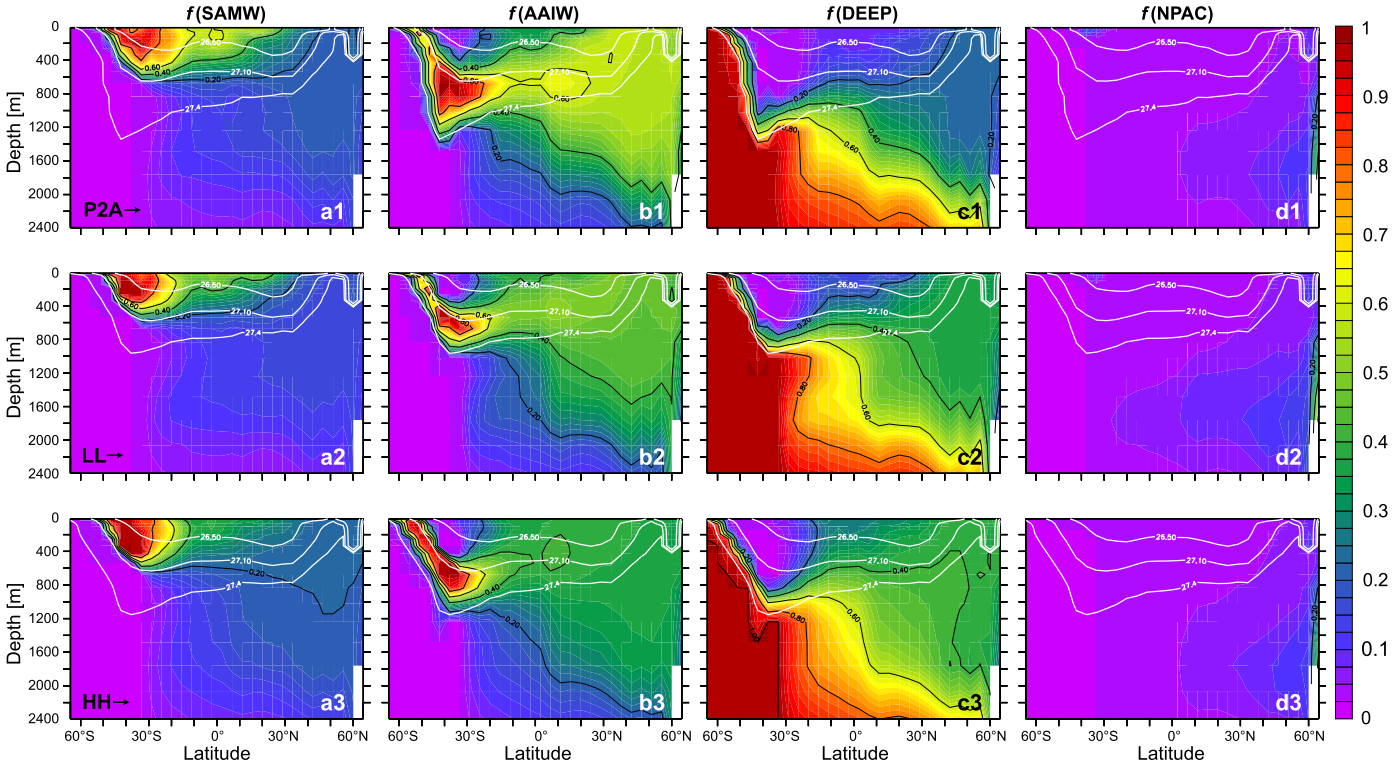

Fig. 7. Meridional section showing the Atlantic-mean contribution of the four source regions to the Si inventory [mol Si/mol Si, unitless] in the uppermost 2400 m of the three model variants. The three white contours correspond to the density horizons used to determine the tagging regions for SAMW- and AAIW-sourced Si (Fig. 4). Fractions are averaged over the Atlantic basin and over the Southern Ocean from 60°W to 30°E.

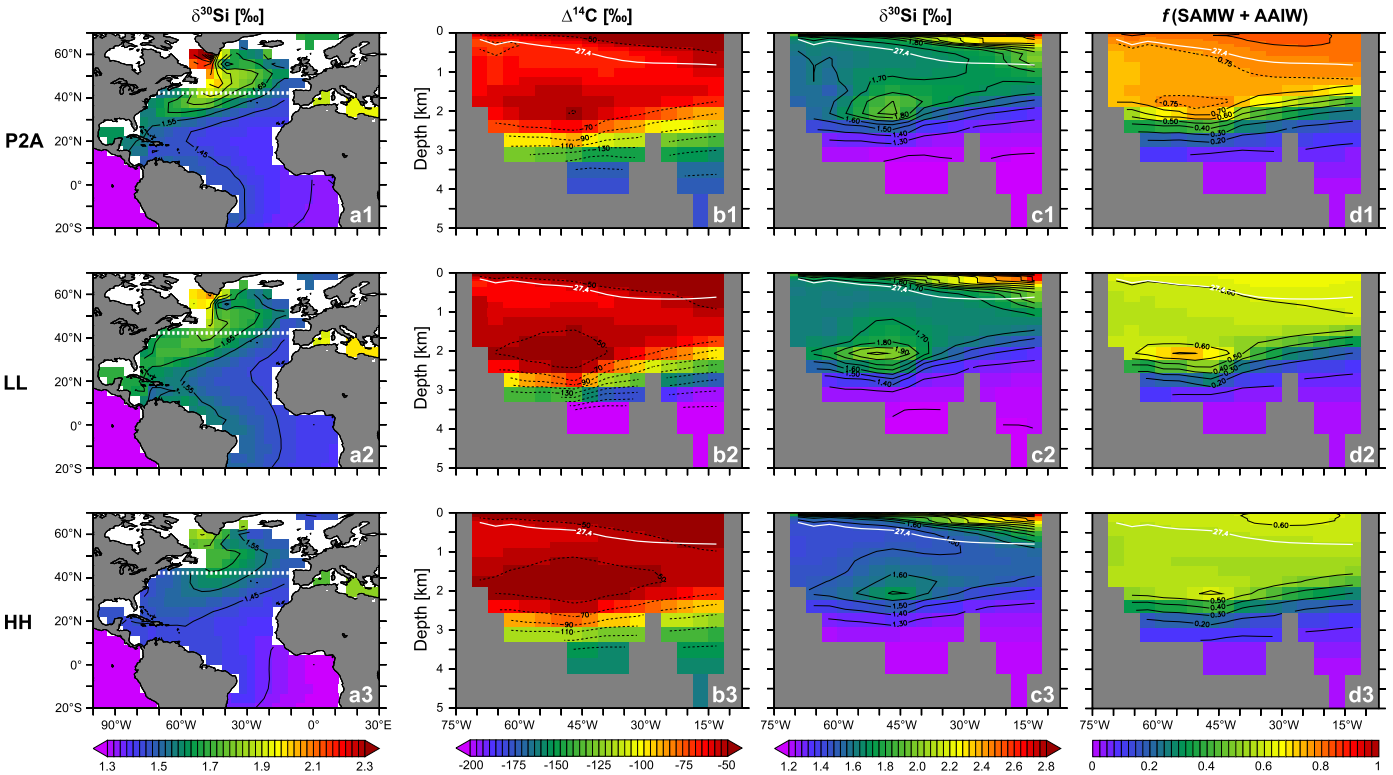

Fig. 8. Isotopic signatures and source composition of NADW in the North Atlantic Ocean. (a) Distribution of δ^{30}Si at ~1700 m water depth, illustrating the southward spreading of the high-δ^{30}Si signature of NADW as a deep western boundary current. The white dotted line at ~43°N in column *a* marks the latitude of the depth sections in columns *b–d*, which show (b) the pre-industrial Δ^{14}C distribution (‰), (c) the δ^{30}Si distribution (‰), and (d) the fractional contribution of SAMW- and AAIW-derived Si to the Si inventory (mol Si/mol Si, unitless).

elevated δ^{30}Si values ranging from +1.7 to +1.9‰ in the western mid-depth North Atlantic (Fig. 1b; de Souza et al., 2012a; Brzezinski and Jones, 2015). Whilst the less diffusive models P2A and LL reproduce the absolute δ^{30}Si values in NADW better than the diffusive model HH (Figs. 8a, c), all three models reproduce the δ^{30}Si systematics of the deep Atlantic with similar fidelity (Fig. 1a), although P2A simulates higher δ^{30}Si values in the subpolar North Atlantic than LL or HH. It is interesting to note that the models reproduce the observed near-linear δ^{30}Si systematics despite the fact that they do not simulate Si isotope fractionation during opal dissolution. This contrasts somewhat with the recent study by Holzer and Brzezinski (2015), who found that including this process improved the linearity of their model's Atlantic δ^{30}Si systematics by increasing δ^{30}Si in the Si-richest Southern Ocean deep waters. Our results and theirs do, however, agree in suggesting that fractionation during opal dissolution is not a major driver of the deep Atlantic δ^{30}Si systematics.

Depth sections across ~43°N reveal the isotopic signal of NADW flowing around the Grand Banks as a well-ventilated water mass: this freshly-ventilated NADW bears a Δ^{14}C maximum (Fig. 8b) and is recognizable in the δ^{30}Si distribution by its elevated δ^{30}Si signature (Fig. 8c) in all models. These isotopic distributions are closely mimicked by the fraction of Si sourced from SAMW and AAIW, f(SAMW + AAIW) (Fig. 8d). The fractional contribution of SAMW- and AAIW-derived Si is highest above the 27.4 isopycnal, in waters flowing towards the high-latitude North Atlantic in the upper limb of the MOC. However, in each model, there is a secondary f(SAMW + AAIW) maximum at mid-depth, coincident with the δ^{30}Si and Δ^{14}C signals of NADW. The fraction of NPAC-derived Si also shows a maximum within this volume, but does not exceed 10% (Fig. S6d). Conversely, DEEP-sourced Si is at its minimum within the freshly-ventilated NADW core (Fig. S6c). Thus, irrespective of the large-scale circulation of the models, there is a clear spatial correlation between the maximum contribution of SAMW- and AAIW-derived Si to NADW and the elevated δ^{30}Si signature observed in the most recently ventilated deep waters (Figs. 8c, d and S7). We can quantify this relationship by calculating the contributions of the source regions to the Si inventory of freshly-ventilated NADW.

Recently ventilated NADW exhibits clear signals of gas exchange with the atmosphere in the models' radiocarbon and oxygen distributions (Figs. 8b, S1 and S2). We exploit these signals to define a volume of freshly-ventilated NADW that extends from the shallow subpolar North Atlantic (>500 m water depth) to the equator along the western Atlantic boundary (Table 1; see also the Supplementary Information). This allows us to calculate the integrated Si inventory of this volume and partition it according to source region (Table 1). In all three model variants, SAMW and AAIW together contribute a major or dominant fraction of the Si inventory, ranging from 46% in HH to 62% in P2A. The importance of DEEP-sourced Si varies inversely with this contribution, whilst NPAC-derived Si is of minor importance (5–9%) in all models.

The δ^{30}Si signature of the freshly-ventilated NADW volume rises systematically with the increase in f(SAMW + AAIW) from HH to P2A, and ranges from +1.50‰ in HH to +1.74‰ in P2A (Table 1). Thus, not only is there a clear spatial correlation between elevated values of f(SAMW+AAIW) and δ^{30}Si *within* each model (Fig. S7), but also systematic co-variation *between* models: the greater the SAMW/AAIW contribution to NADW, the higher its δ^{30}Si value. Together, these correlations strongly suggest that cross-equatorial transport of Si that has been isotopically fractionated in the surface Southern Ocean is instrumental in producing the high δ^{30}Si signature of NADW.

Table 1
Quantification of Si source contributions to freshly-ventilated NADW. Threshold values of Δ^{14}C and [O_2] used to define the volume of freshly-ventilated North Atlantic Deep Water (see Supplementary Information) in the model variants used in this study, together with integrated δ^{30}Si signature and contributions of the four source regions to the Si inventory of this volume.

	HH	LL	P2A
Radiocarbon threshold [‰]	−70	−70	−80
Oxygen threshold [mmol/m^3]	260	260	240
Properties of the NADW volume:			
NADW δ^{30}Si [‰]	**+1.50**	**+1.66**	**+1.74**
f(SAMW)	0.166	0.124	0.267
f(AAIW)	0.292	0.368	0.348
***f*(*SAMW* + *AAIW*)**	***0.457***	***0.491***	***0.615***
f(DEEP)	0.484	0.419	0.331
f(NPAC)	0.059	0.090	0.054
Source-region isotope signatures:			
SAMW δ^{30}Si [‰]	+1.71	+2.07	+2.31
AAIW δ^{30}Si [‰]	+1.37	+1.47	+1.52
DEEP δ^{30}Si [‰]	+1.19	+1.18	+1.15
NPAC δ^{30}Si [‰]	+1.62	+1.66	+1.57
Source-region signature propagation (Eqn. (1)):			
NADW $\delta^{30}Si_{distal}$ [‰]	**+1.35**	**+1.44**	**+1.61**
NADW $\delta^{30}Si_{distal}$ − NADW δ^{30}Si [‰]	−0.14	−0.22	−0.13
Deep Atlantic δ^{30}Si gradient:			
AABW δ^{30}Si [‰]	+1.18	+1.16	+1.10
NADW δ^{30}Si − AABW δ^{30}Si [‰]	0.31	0.50	0.64
NADW $\delta^{30}Si_{distal}$ − AABW δ^{30}Si [‰]	0.17	0.28	0.51
Fraction of δ^{30}Si difference explained by $\delta^{30}Si_{distal}$	**54%**	**56%**	**80%**

4.2. Distal and proximal fractionation controls on the NADW δ^{30}Si signature

The elevated δ^{30}Si signal of NADW is reproduced by all three models, despite their widely varying MOC configurations. Whilst the analysis above indicates that this signal derives from the contribution of SAMW/AAIW to NADW's Si inventory, we must also consider two additional factors that can produce differences in the NADW δ^{30}Si signature between model variants. These are: (a) the isotopic composition of Si exported from each source region, and (b) Si isotope fractionation at the ocean's surface during transport from the source regions to the North Atlantic. In other words, the NADW δ^{30}Si signature can be conceived of as resulting from a combination of the *conservative* transport of isotope signatures from distal source regions, and the *non-conservative* alteration of these isotope signatures en route. We can separate the effects of these two factors with a simple isotope mixing calculation, allowing us to assess the extent to which the NADW δ^{30}Si signature is controlled by the conservative transport of distal isotopic signals. We calculate the isotopic composition of Si within each source region (Table 1) as an estimate of the distal isotopic signals being exported towards the North Atlantic. Based on these values and the source tracer contributions at each model grid point, we can then calculate the δ^{30}Si distribution that would result simply from the spreading of these endmember δ^{30}Si signatures:

$$\delta^{30}Si_{distal} = \sum_i f(i) \cdot \delta^{30}Si_{i,source} \quad (1)$$

where $f(i)$ is the local fractional contribution of the source i, and $\delta^{30}Si_{i,source}$ is the isotopic composition in the source region i. We hasten to note that this approach makes the simplifying assumption that Si supplied from each source region has a uniform δ^{30}Si value, which is not the case. However, as we show below, it nonetheless serves to provide us with a useful estimate of the influence of the large-scale transport of isotope signals.

The meridional sections in Fig. 9 compare the simulated Atlantic δ^{30}Si distribution at 25°W (Fig. 9a) with the $\delta^{30}Si_{distal}$ dis-

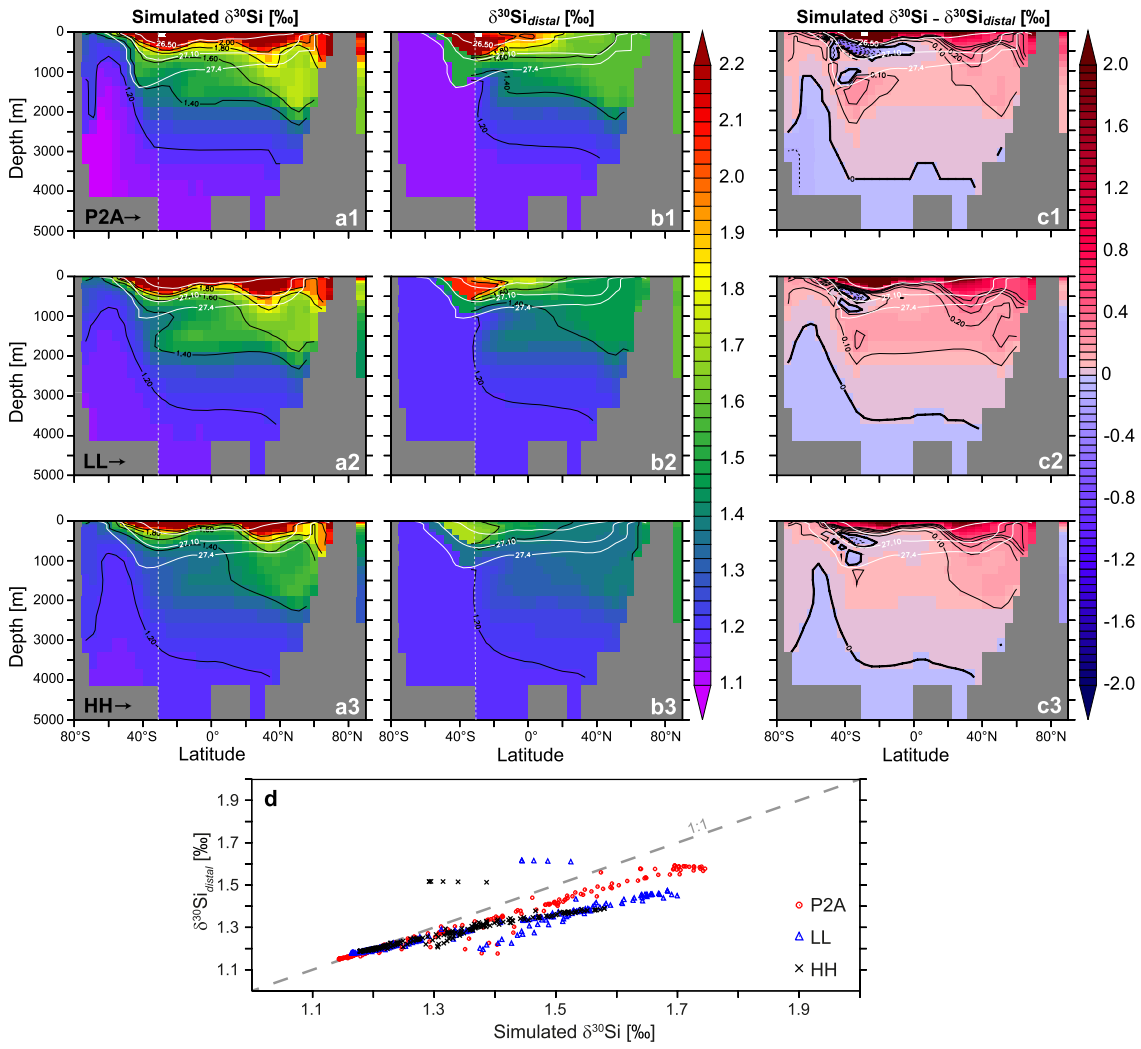

Fig. 9. Meridional sections at 25°W in the Atlantic Ocean from all three model variants, comparing (a) the simulated δ^{30}Si distribution with (b) the $\delta^{30}Si_{distal}$ distribution calculated using Eqn. (1), i.e. the δ^{30}Si distribution expected simply from propagation of source-region δ^{30}Si signatures. Panel *c* shows the difference between panels *a* and *b*. White solid lines are isopycnal surfaces used in the definition of *SAMW* and *AAIW* tagging regions (Fig. 4); the white dotted line marks 30°S, the northernmost extent of the *DEEP* tagging region. In panel *d*, a scatterplot directly compares the deep $\delta^{30}Si_{distal}$ distribution (>1000 m) to the simulated δ^{30}Si distribution north of 30°S, illustrating both the clear correlation between the two fields as well as the muted dynamic range of $\delta^{30}Si_{distal}$.

tribution (Fig. 9b). It can be seen that in all three model variants, considerable large-scale interior Atlantic δ^{30}Si variability, including an elevated NADW δ^{30}Si signature, is predicted to result simply from the propagation of distal source-region δ^{30}Si signals. Furthermore, as shown by the close correlation between the two fields (Fig. 9d), the structure of the $\delta^{30}Si_{distal}$ distribution bears a strong resemblance to the simulated δ^{30}Si field. These results indicate that the long-range transport of isotope signals plays a significant role in determining the basin-scale δ^{30}Si distribution. However, in all cases the range in $\delta^{30}Si_{distal}$ is muted in comparison to the simulated field (slopes <1 in Fig. 9d), with $\delta^{30}Si_{distal}$ values generally lower than simulated values in the upper ocean (Fig. 9c). This is reflected in the $\delta^{30}Si_{distal}$ signature of the freshly-ventilated NADW volume, which underestimates the simulated δ^{30}Si value by 0.13–0.22‰ (Table 1).

Two reasons for the mismatch between $\delta^{30}Si_{distal}$ and simulated δ^{30}Si become clear upon closer inspection of Fig. 9. Firstly, the assumption of uniform source δ^{30}Si values in Eqn. (1) ignores the significant isotopic variability within each source region. This simplification results, for example, in the northward propagation of too-low $\delta^{30}Si_{distal}$ values from the Southern Ocean just below the $\sigma_\theta = 27.4$ isopycnal in all models, reflected by the bolus of elevated mismatch at this location in all models (Fig. 9c). Secondly, a clear difference between δ^{30}Si and $\delta^{30}Si_{distal}$ is observed in the near-surface ocean, where the simulated δ^{30}Si field exhibits high values throughout the low latitudes and in the subpolar North Atlantic (Fig. 9a), whilst $\delta^{30}Si_{distal}$ values in the uppermost 500 m decrease considerably from the southern tropics northwards (Fig. 9b). This change is seen mostly clearly at the level of SAMW in all models (Fig. 9c), where the sign of mismatch between the two fields changes from negative ($\delta^{30}Si_{distal} > \delta^{30}$Si) to positive ($\delta^{30}$Si $> \delta^{30}Si_{distal}$) towards the north. The decoupling of $\delta^{30}Si_{distal}$ from δ^{30}Si during northward transport in the upper ocean is the result of two opposing tendencies. A decrease in $\delta^{30}Si_{distal}$ is driven by the upward transport of AAIW- and DEEP-sourced Si in the low-latitude ocean (Figs. 7 and 8), pools that have significantly lower δ^{30}Si values than SAMW-sourced Si (Table 1). In contrast, an elevation of simulated δ^{30}Si values in the upper ocean results from isotope fractionation during Si utilization in the low latitude ocean and the subpolar North Atlantic. This fractionation directly affects δ^{30}Si values in the surface ocean, but also more indirectly elevates near-surface δ^{30}Si via the subduction of a high-δ^{30}Si signal into the subtropical North Atlantic thermocline. Thus, some fraction of the difference between the δ^{30}Si and $\delta^{30}Si_{distal}$ fields results from the isotope fractionation of Si within the Atlantic Ocean.

This result implies that the elevated NADW δ^{30}Si signature simulated by the models is not simply the result of distal fractionation in the surface Southern Ocean, but also reflects more proximal isotope fractionation as Si is transported towards the NADW formation region in the upper limb of the MOC, i.e. the *non-conservative* effect discussed above. The offset between the δ^{30}Si and $\delta^{30}Si_{distal}$ fields is much smaller at the depth of NADW than in the upper ocean (Fig. 9a, b), showing that the signal of proximal fractionation is damped during NADW formation. This is due to the importance of Si-richer subsurface waters, whose Si inventory is not exposed to isotope fractionation in the surface, in determining the NADW δ^{30}Si value (cf. Sigman et al., 2000).

Due to the uncertainty introduced into our calculation of $\delta^{30}Si_{distal}$ by the assumption of constant source region δ^{30}Si signatures, we can only provide an estimate of the extent of the proximal modulation of distal isotope signals. A useful metric for this estimation is the deep Atlantic δ^{30}Si gradient, i.e. the difference between the δ^{30}Si values of NADW and AABW. The three model variants produce Atlantic deep water δ^{30}Si differences of varying strength, ranging from 0.31‰ in HH to 0.63‰ in P2A (Table 1), compared to an observed difference of $\sim$ 0.5‰ (de Souza et al., 2012a). By assessing what proportion of this basin-scale δ^{30}Si difference is explained by the $\delta^{30}Si_{distal}$ signature of NADW, we can estimate the fraction that results simply from the propagation of source-region δ^{30}Si signatures. The results shown in Table 1 reveal that this conservative effect explains 54% to 80% of the deep Atlantic δ^{30}Si gradient. Our simulations thus indicate that the high δ^{30}Si value of NADW, and indeed the basin-scale δ^{30}Si distribution, is largely governed by the transport of distal surface Southern Ocean isotope signatures to the North Atlantic in SAMW and AAIW, as postulated by de Souza et al. (2012a).

4.3. Compensatory mechanisms in the Atlantic δ^{30}Si systematics

The above discussion of the distal and proximal controls on the δ^{30}Si distribution also helps elucidate the mechanisms by which the models all produce an elevated NADW δ^{30}Si signal, despite differing pathways of deep water upwelling. The importance of the cross-equatorial transport of distal isotopic signals in producing the Atlantic δ^{30}Si gradient differs between the models, and is least in the highly diffusive model HH, which upwells more interior Si to the surface in the low latitudes (Table 1). This relationship suggests that there are compensatory mechanisms at play in the models' Atlantic δ^{30}Si systematics: the more diffusive model HH advects less fractionated Si to the North Atlantic from the surface Southern Ocean (Figs. 6–8), but produces a high-δ^{30}Si signal more proximally through fractionation of more vigorously supplied deeply-sourced Si in the low-latitude or subarctic Atlantic (Fig. 9), allowing it to produce NADW with a high δ^{30}Si value. Conversely, the more adiabatic models P2A and LL favour distal control on the elevated δ^{30}Si of NADW. The models thus trade off between distal and proximal isotope fractionation as a means of supplying isotopically fractionated Si to the NADW formation region. It is this compensation that allows all three models to produce Atlantic δ^{30}Si systematics that are remarkably similar to observations (Fig. 1a), despite their widely-varying MOC pathways. The existence of these interacting controls on the NADW δ^{30}Si signature also means that the presence of an Atlantic δ^{30}Si gradient cannot be uniquely tied to fractionation in the high-latitude Southern Ocean, as suggested by de Souza et al. (2012a). As a result, our simulations indicate that this isotopic feature does not constrain the pathways by which deep water is returned to the upper ocean in the MOC.

More generally, the results of our study contribute to an emerging picture of the role of Southern Ocean Si isotope "distillation" (Brzezinski and Jones, 2015) in governing the marine δ^{30}Si distribution. This distillation results from the combined physical and biogeochemical dynamics of the Southern Ocean, and leads to the trapping of low-δ^{30}Si silicic acid in the deep Southern Ocean (Holzer et al., 2014; Holzer and Brzezinski, 2015) coupled to a complementary northward export of a high-δ^{30}Si signature in SAMW/AAIW (Fripiat et al., 2011; de Souza et al., 2012b). de Souza et al. (2014) have recently shown that the isotopically light preformed and regenerated Si in the deep Southern Ocean is spread throughout the global abyssal ocean by AABW, producing the observed hydrographic control on the deep δ^{30}Si distribution. This study has highlighted the large-scale influence of the complementary high δ^{30}Si signal exported in SAMW/AAIW, showing that the Southern Ocean influences the global δ^{30}Si distribution by two separate pathways associated with the upper *and* lower limbs of the MOC. However, consistent with the recent study by Holzer and Brzezinski (2015), our results also allow a role for fractionation during low-latitude Si cycling in determining the large-scale δ^{30}Si distribution, indicating that other ocean regions may modulate the signals exported from the Southern Ocean.

An important open question that our study does not explicitly address is the role of the Arctic Ocean, which Brzezinski and Jones (2015) have suggested may represent an important northern counterpart to the Southern Ocean, via its influence on the Nordic Sea overflows. The Arctic Ocean receives fractionated Si primarily through shallow inflow from the North Atlantic, and transfers this Si to deep-water densities via buoyancy loss (Jones et al., 1995). Certainly some of the SAMW/AAIW-sourced Si in our models' NADW has been incorporated in this manner. What remains to be assessed is whether the Arctic Ocean's role is limited to such diapycnal Si transfer, or whether a significant additional fractionation signal is imposed by Si cycling within the Arctic itself. Answering this question will require the long-overdue analysis of the Arctic δ^{30}Si distribution.

5. Conclusions

This study has combined models of the marine cycle of Si and its isotopes with a diagnostic scheme that enables us to trace the large-scale transport of Si originating from the high-latitude ocean in a suite of OGCM simulations with varying MOC pathways. These simulations allow an assessment of the role of cross-equatorial transport of SAMW- and AAIW-derived Si in producing the elevated δ^{30}Si signature of NADW. We find that Si sourced from the SAMW and AAIW formation regions contributes a major to dominant fraction (46–62%) of the freshly-ventilated NADW Si inventory irrespective of MOC pathway, and that the δ^{30}Si signature of NADW rises as the contribution of SAMW- and AAIW-derived Si increases. However, the simulations also indicate that more proximal isotope fractionation of Si, within the low-latitude or subpolar North Atlantic, can influence the NADW δ^{30}Si signature. By revealing this interplay between distal and proximal processes, our results thus allow us to refine the hypothesis of de Souza et al. (2012a): the high δ^{30}Si signature of NADW is vitally linked to the transport of a fractionated signal from the surface Southern Ocean by SAMW/AAIW, but may also be additionally influenced by Si isotope fractionation that takes place during transport to the NADW formation region. The more adiabatic models in our suite, which conform best to our current understanding of deep-water upwelling pathways (e.g. Talley, 2013), suggest that the proximal contribution is small, although definitive conclusions remain elusive given lingering uncertainties regarding the pathways of the MOC (e.g. Talley, 2008).

Acknowledgements

The authors gratefully acknowledge helpful comments on an earlier version of this manuscript by Timothy Conway and Beat-

rice Radden Keefe, and the constructive reviews of two anonymous reviewers. This work was supported by Swiss National Science Foundation post-doctoral fellowships PBEZP2-140169 and P300P2-147747 granted to GFDS, NOAA grant NA11OAR4310066 to JLS, and UK NERC grant NE/K00901X/1 to MPH.

Appendix A. Supplementary material

Supplementary material related to this article can be found online at http://dx.doi.org/10.1016/j.epsl.2015.10.025.

References

Abouchami, W., Galer, S.J.G., de Baar, H.J.W., Middag, R., Vance, D., Zhao, Y., et al., 2014. Biogeochemical cycling of cadmium isotopes in the Southern Ocean along the Zero Meridian. Geochim. Cosmochim. Acta 127, 348–367.

Beucher, C.P., Brzezinski, M.A., Jones, J.L., 2008. Sources and biological fractionation of Silicon isotopes in the Eastern Equatorial Pacific. Geochim. Cosmochim. Acta 72, 3063–3073.

Broecker, W.S., Peng, T.H., 1982. Tracers in The Sea. Eldigio Press/Lamont-Doherty Geological Observatory, Palisades, NY.

Broecker, W.S., Blanton, S., Smethie, W.M., Ostlund, G., 1991. Radiocarbon decay and oxygen utilization in the deep Atlantic Ocean. Glob. Biogeochem. Cycles 5, 87–117.

Brzezinski, M.A., Dickson, M.L., Nelson, D.M., Sambrotto, R., 2003. Ratios of Si, C and N uptake by microplankton in the Southern Ocean. Deep-Sea Res. II 50, 619–633.

Brzezinski, M.A., Jones, J.L., 2015. Coupling of the distribution of silicon isotopes to the meridional overturning circulation of the North Atlantic Ocean. Deep-Sea Res. II 116, 79–88.

Buesseler, K.O., 1998. The decoupling of production and particulate export in the surface ocean. Glob. Biogeochem. Cycles 12, 297–310.

Cardinal, D., Alleman, L.Y., Dehairs, F., Savoye, N., Trull, T.W., Andre, L., 2005. Relevance of silicon isotopes to Si-nutrient utilization and Si-source assessment in Antarctic waters. Glob. Biogeochem. Cycles 19. http://dx.doi.org/10.1029/2004GB002364.

De La Rocha, C.L., Brzezinski, M.A., DeNiro, M.J., 1997. Fractionation of silicon isotopes by marine diatoms during biogenic silica formation. Geochim. Cosmochim. Acta 61, 5051–5056.

Demarest, M.S., Brzezinski, M.A., Beucher, C.P., 2009. Fractionation of silicon isotopes during biogenic silica dissolution. Geochim. Cosmochim. Acta 73, 5572–5583.

de Souza, G.F., Reynolds, B.C., Rickli, J., Frank, M., Saito, M.A., Gerringa, L.J.A., et al., 2012a. Southern Ocean control of silicon stable isotope distribution in the deep Atlantic Ocean. Glob. Biogeochem. Cycles 26. http://dx.doi.org/10.1029/2011gb004141.

de Souza, G.F., Reynolds, B.C., Johnson, G.C., Bullister, J.L., Bourdon, B., 2012b. Silicon stable isotope distribution traces Southern Ocean export of Si to the eastern South Pacific thermocline. Biogeosciences 9, 4199–4213.

de Souza, G.F., Slater, R.D., Dunne, J.P., Sarmiento, J.L., 2014. Deconvolving the controls on the deep ocean's silicon stable isotope distribution. Earth Planet. Sci. Lett. 398, 66–76.

Fripiat, F., Cavagna, A.-J., Dehairs, F., Speich, S., André, L., Cardinal, D., 2011. Silicon pool dynamics and biogenic silica export in the Southern Ocean, inferred from Si-isotopes. Ocean Sci. 7, 533–547.

Garcia, H.E., Locarnini, R.A., Boyer, T.P., Antonov, J.I., 2010. World Ocean Atlas 2009, Volume 4: Nutrients (Phosphate, Nitrate, Silicate). U.S. Government Printing Office, Washington, DC.

Gent, P.R., Willebrand, J., McDougall, T.J., McWilliams, J.C., 1995. Parametrizing eddy-induced tracer transports in ocean circulation models. J. Phys. Oceanogr. 25, 463–474.

Gnanadesikan, A., 1999. A simple predictive model for the structure of the oceanic pycnocline. Science 283, 2077–2079.

Gnanadesikan, A., Slater, R.D., Gruber, N., Sarmiento, J.L., 2002. Oceanic vertical exchange and new production: a comparison between models and observations. Deep-Sea Res. II 49, 363–401.

Gnanadesikan, A., Dunne, J., Key, R., Matsumoto, K., Sarmiento, J.L., Slater, R., et al., 2004. Oceanic ventilation and biogeochemical cycling: understanding the physical mechanisms that produce realistic distributions of tracers and productivity. Glob. Biogeochem. Cycles 18. http://dx.doi.org/10.1029/2003GB002097.

Gnanadesikan, A., De Boer, A.M., Mignone, B.K., 2007. A simple theory of the pycnocline and overturning revisited. In: Schmittner, A., Chiang, J.C.H., Hemming, S. (Eds.), Ocean Circulation: Mechanisms and Impacts—Past and Future Changes of Meridional Overturning. American Geophysical Union, pp. 19–32.

Gordon, A.L., 1986. Interocean exchange of thermocline water. J. Geophys. Res., Oceans 91, 5037–5046.

Grasse, P., Ehlert, C., Frank, M., 2013. The influence of water mass mixing on the dissolved Si isotope composition in the Eastern Equatorial Pacific. Earth Planet. Sci. Lett. 380, 60–71.

Hain, M.P., Sigman, D.M., Haug, G.H., 2014a. The biological pump in the past. In: Holland, H., Turekian, K.K. (Eds.), Treatise on Geochemistry, second ed.. Elsevier, Amsterdam, pp. 485–517.

Hain, M.P., Sigman, D.M., Haug, G.H., 2014b. Distinct roles of the Southern Ocean and North Atlantic in the deglacial atmospheric radiocarbon decline. Earth Planet. Sci. Lett. 394, 198–208.

Hellerman, S., Rosenstein, M., 1983. Normal monthly wind stress over the world ocean with error estimates. J. Phys. Oceanogr. 13, 1093–1104.

Holzer, M., Primeau, F.W., DeVries, T., Matear, R., 2014. The Southern Ocean silicon trap: data-constrained estimates of regenerated silicic acid, trapping efficiencies, and global transport paths. J. Geophys. Res., Oceans 119. http://dx.doi.org/10.1002/2013jc009356.

Holzer, M., Brzezinski, M.A., 2015. Controls on the silicon isotope distribution in the ocean: new diagnostics from a data-constrained model. Glob. Biogeochem. Cycles 29. http://dx.doi.org/10.1002/2014GB004967.

Jin, X., Gruber, N., Dunne, J.P., Sarmiento, J.L., Armstrong, R.A., 2006. Diagnosing the contribution of phytoplankton functional groups to the production and export of particulate organic carbon, $CaCO_3$, and opal from global nutrient and alkalinity distributions. Glob. Biogeochem. Cycles 20. http://dx.doi.org/10.1029/2005GB002532.

Jones, E.P., Rudels, B., Anderson, L.G., 1995. Deep waters of the Arctic Ocean: origins and circulation. Deep-Sea Res. I 42, 737–760.

Karleskind, P., Lévy, M., Memery, L., 2011. Subduction of carbon, nitrogen, and oxygen in the northeast Atlantic. J. Geophys. Res., Oceans 116. http://dx.doi.org/10.1029/2010jc006446.

Keir, R.S., 1988. On the Late Pleistocene ocean geochemistry and circulation. Paleoceanography 3, 413–455.

Ledwell, J.R., Watson, A.J., Law, C.S., 1993. Evidence for slow mixing across the pycnocline from an open-ocean tracer-release experiment. Nature 364, 701–703.

Ledwell, J.R., Watson, A.J., Law, C.S., 1998. Mixing of a tracer in the pycnocline. J. Geophys. Res., Oceans 103, 21,499–21,529.

Lumpkin, R., Speer, K., 2007. Global ocean meridional overturning. J. Phys. Oceanogr. 37, 2550–2562.

Marinov, I., Gnanadesikan, A., Toggweiler, J.R., Sarmiento, J.L., 2006. The Southern Ocean biogeochemical divide. Nature 441, 964–967.

Marshall, J., Speer, K., 2012. Closure of the meridional overturning circulation through Southern Ocean upwelling. Nat. Geosci. 5, 171–180.

Matsumoto, K., Sarmiento, J.L., Key, R.M., Aumont, O., Bullister, J.L., Caldeira, K., et al., 2004. Evaluation of ocean carbon cycle models with data-based metrics. Geophys. Res. Lett. 31. http://dx.doi.org/10.1029/2003gl018970.

Morrison, A.K., Fröhlicher, T.L., Sarmiento, J.L., 2015. Upwelling in the Southern Ocean. Phys. Today 68. http://dx.doi.org/10.1063/PT.1063.2654.

Pacanowski, R.C., Griffies, S.M., 1999. The MOM3 Manual. NOAA/Geophysical Fluid Dynamics Laboratory, Princeton.

Palter, J.B., Lozier, M.S., Barber, R.T., 2005. The effect of advection on the nutrient reservoir in the North Atlantic subtropical gyre. Nature 437, 687–692.

Palter, J.B., Sarmiento, J.L., Gnanadesikan, A., Simeon, J., Slater, R.D., 2010. Fueling export production: nutrient return pathways from the deep ocean and their dependence on the meridional overturning circulation. Biogeosciences 7, 3549–3568.

Palter, J.B., Lozier, M.S., Sarmiento, J.L., Williams, R.G., 2011. The supply of excess phosphate across the Gulf Stream and the maintenance of subtropical nitrogen fixation. Glob. Biogeochem. Cycles 25. http://dx.doi.org/10.1029/2010GB003955.

Polzin, K.L., Toole, J.M., Ledwell, J.R., Schmitt, R.W., 1997. Spatial variability of turbulent mixing in the abyssal ocean. Science 276, 93–96.

Raven, J.A., 1983. The transport and function of silicon in plants. Biol. Rev. 58, 179–207.

Reynolds, B.C., Frank, M., Halliday, A.N., 2006. Silicon isotope fractionation during nutrient utilization in the North Pacific. Earth Planet. Sci. Lett. 244, 431–443.

Robinson, A., Stommel, H., 1959. The oceanic thermocline and the associated thermohaline circulation. Tellus 11, 295–308.

Robinson, R.S., Sigman, D.M., DiFiore, P.J., Rohde, M.M., Mashiotta, T.A., Lea, D.W., 2005. Diatom-bound $^{15}N/^{14}N$: new support for enhanced nutrient consumption in the ice age Subantarctic. Paleoceanography 20. http://dx.doi.org/10.1029/2004pa001114.

Sarmiento, J.L., Gruber, N., Brzezinski, M.A., Dunne, J.P., 2004. High-latitude controls of thermocline nutrients and low latitude biological productivity. Nature 427, 56–60.

Sarmiento, J.L., Simeon, J., Gnanadesikan, A., Gruber, N., Key, R.M., Schlitzer, R., 2007. Deep ocean biogeochemistry of silicic acid and nitrate. Glob. Biogeochem. Cycles 21. http://dx.doi.org/10.1029/2006GB002720.

Sallée, J.-B., Speer, K., Rintoul, S., Wijffels, S., 2010. Southern Ocean thermocline ventilation. J. Phys. Oceanogr. 40, 509–529.

Sigman, D.M., Altabet, M.A., McCorkle, D.C., François, R., Fischer, G., 2000. The $\delta^{15}N$ of nitrate in the Southern Ocean: nitrogen cycling and circulation in the ocean interior. J. Geophys. Res., Oceans 105, 19599–19614.

Smetacek, V., 1999. Diatoms and the ocean carbon cycle. Protist 150, 25–32.

Sutton, J.N., Varela, D.E., Brzezinski, M.A., Beucher, C.P., 2013. Species-dependent silicon isotope fractionation by marine diatoms. Geochim. Cosmochim. Acta 104, 300–309.

Talley, L.D., 2008. Freshwater transport estimates and the global overturning circulation: shallow, deep and throughflow components. Prog. Oceanogr. 78, 257–303.

Talley, L.D., 2013. Closure of the global overturning circulation through the Indian, Pacific, and Southern Oceans: schematics and transports. Oceanography 26, 80–97.

Talley, L.D., Reid, J.L., Robbins, P.E., 2003. Data-based meridional overturning streamfunctions for the global ocean. J. Climate 16, 3213–3226.

Toggweiler, J.R., Samuels, B., 1993. New radiocarbon constraints on the upwelling of abyssal water to the ocean's surface. In: Heimann, M. (Ed.), The Global Carbon Cycle. Springer, Berlin, pp. 333–366.

Tréguer, P.J., De La Rocha, C.L., 2013. The world ocean silica cycle. Ann. Rev. Mar. Sci. 5, 477–501.

Trenberth, K.E., Olson, J., Large, W., 1989. A global ocean wind stress climatology based on ECMWF analyses. Technical Report NCAR/TN-338+STR. National Center for Atmospheric Research, Boulder, CO.

Wetzel, F., de Souza, G.F., Reynolds, B.C., 2014. What controls silicon isotope fractionation during dissolution of diatom opal? Geochim. Cosmochim. Acta 131, 128–137.